



DOI: 10.29026/oea.2020.190022

# Ultrasensitive skin-like wearable optical sensors based on glass micro/nanofibers

Lei Zhang<sup>1\*</sup>, Jing Pan<sup>1</sup>, Zhang Zhang<sup>1</sup>, Hao Wu<sup>1</sup>, Ni Yao<sup>1</sup>, Dawei Cai<sup>1</sup>, Yingxin Xu<sup>1</sup>, Jin Zhang<sup>1</sup>, Guofei Sun<sup>2</sup>, Liqiang Wang<sup>1</sup>, Weidong Geng<sup>2</sup>, Wenguang Jin<sup>3</sup>, Wei Fang<sup>1</sup>, Dawei Di<sup>1,4</sup> and Limin Tong<sup>1\*</sup>

<sup>1</sup>State Key Laboratory of Modern Optical Instrumentation, College of Optical Science and Engineering, Zhejiang University, Hangzhou 310027, China; <sup>2</sup>College of Computer Science and Technology, Zhejiang University, Hangzhou 310027, China; <sup>3</sup>College of Information Science and Electronic Engineering, Zhejiang University, Hangzhou 310027, China; <sup>4</sup>Cavendish Laboratory, University of Cambridge, JJ Thomson Avenue, Cambridge CB3 0HE, United Kingdom.

\*Correspondence: L Zhang, E-mail: lei\_zhang@zju.edu.cn; L M Tong, E-mail: phytong@zju.edu.cn

## This file includes:

Section 1: Fabrication of MNFs

Section 2: Manipulation of the as-fabricated MNFs

Section 3: Fabrication of SLWOS on solid substrate

Section 4: Fabrication of suspended SLWOS

Section 5: Simulating the bending loss of the PDMS embedded MNF

Section 6: Measuring the additional optical loss of an MNF caused by PDMS embedding

Section 7: Modeling the power distribution outside the MNF

Section 8: Calculating the sensitivity and detection limit of the SLWOS

Section 9: Measuring response time of a SLWOS

Section 10: Characterization of data glove and SLWOSs embedded with 2×2 MNF arrays

Fig. S1–Fig. S7

Table S1–Table S2

Movie S1–Movie S3

Supplementary information for this paper is available at <https://doi.org/10.29026/oea.2020.190022>

### Section 1: Fabrication of MNFs

The MNFs were fabricated by stretching a standard glass optical fiber using a home-built taper drawing system<sup>1</sup> as shown in Fig. S1. A hydrogen flame was used to heat the fiber to its softening temperature. To precisely control the heating temperature, the hydrogen gas flow (115 ml/min) was controlled by a digital mass flow controller (CS200, Sevenstar). The standard optical fiber (SMF28e or 62.5/125, Corning Inc.) was fixed on fiber clamps and preheated for ~100 seconds before being stretched by two computer controlled high-precision translation stages (ESP301, Newport) at a velocity of 0.1 mm/s. Under a certain pulling force, the fiber was stretched and elongated gradually with reduced diameter until the desired length or diameter was reached. During the fiber stretching process, a 785-nm-wavelength light was coupled to the fiber, and transmission was measured by a photo detector (918D-UV-OD3R, Newport). With this system, a biconically tapered fiber could be fabricated with a uniform waist (i.e., MNF), desired diameter down to 500 nm and length up to 10 cm. The measured overall transmission can typically go up to 95%.

### Section 2: Manipulation of the as-fabricated MNFs

Using scanning tunneling microscope (STM) probes or tapered fiber probes, the as-fabricated MNF can be positioned, bent, and twisted with high precision under an optical microscope. In this work, the as-fabricated MNFs were positioned on a PDMS film with desired structures (see Fig. 1(e) for example). When the MNFs were placed on a solid or elastic substrate, they were held tightly in place by the van der Waals attraction between the MNFs and the substrate. If necessary, the MNFs can be picked up and repositioned using a STM probe controlled by a 3-D stage (PT3, Thorlabs) under a stereo microscope (SMZ18, Nikon).

### Section 3: Fabrication of SLWOS on solid substrate

Typically, a SLWOS was fabricated by using a three-step procedure. **Step 1:** Preparing PDMS film. Degassed PDMS (Base : Curing agent = 10:1) was poured onto a glass slide to form a uniform coating, followed by heating to 80 °C for 20 minutes to cure the PDMS. The thickness of the PDMS can be well controlled from 30 μm to 1 mm by the volume of the PDMS or the speed of a spin coater. As a typical case, when 0.4 mL of degassed PDMS was poured onto a glass slide (7.62 cm × 2.54 cm), the thickness of a PDMS film was about 200 μm. To prepare thinner PDMS film, a spin coater was used to reduce the thickness of the PDMS coating. For reference, a spin coating with speed of 1000 rpm and time of 30 s yielded a PDMS film with a thickness of 80 μm. **Step 2:** Placing the MNF on the surface of the PDMS film with micromanipulation under a stereo microscope. **Step 3:** Embedding the MNF. The MNFs on the PDMS film were enclosed by a second PDMS film brushing-coated with a micrometer-thickness degassed PDMS, followed by heating to 80 °C for 20 minutes. The as-fabricated SLWOS can be peeled off from the glass slide and pasted onto objective structures such as skin (Fig. 1(d)) or glove (Fig. 4(a)).

### Section 4: Fabrication of suspended SLWOS

Different from the fabrication of SLWOS on solid substrate, a suspended SLWOS as shown in Fig. 3(a) was prepared by using a four-step procedure. **Step 1:** Preparing PDMS supporting terraces. Degassed PDMS (2 mL in volume) was poured onto a glass slide (7.62 cm × 2.54 cm), followed by heating to 80 °C for 20 minutes to form a layer of 1-mm-thickness PDMS. Cut the PDMS layer with a sharp razor to form two 25-mm-square terraces with 5-mm-gap apart. **Step 2:** Suspended a thin PDMS film across the gap. **Step 3:** Placed an MNF on the PDMS film with input/output fibers supported by the terraces. **Step 4:** Embedding the MNF. Brushing a thin layer of PDMS (e.g. 5 μm) on the suspended MNF-PDMS film, followed by heating to 80 °C for 20 minutes.

The SLWOS for wrist pulse sensing was fabricated by using a modified procedure. Instead of cutting into terraces, a 3-mm-diameter hole was punched on the 1-mm-thickness PDMS layer, and was covered by a thin PDMS film (e.g., 0.5 cm × 0.5 cm, 80 μm in thickness). Then, an MNF was placed on the PDMS film with a U-shape as shown in the inset of Fig. 3(f), brushed a thin layer of PDMS (e.g., 5 μm), and cured at 80 °C for 20 minutes. For wrist pulse sensing, the SLWOS was pasted on the wrist with the suspended film right above the radial artery.

### Section 5: Simulating the bending loss of the PDMS embedded MNF

We theoretically simulated bending losses of PDMS-embedded MNFs using a three-dimensional finite-difference time-domain (3D-FDTD) method<sup>2</sup>, which has been proved efficient and widely employed for simulating optical waveguiding behavior in high-index-contrast waveguides, MNFs and nanowires. For slight bending, here we assume a typical case of circular bending with a bending angle of 5°, as shown in Fig. 2(b). The simulation was performed with MNF diameter of 1 μm, wavelength of the probing light of 900 nm, and indices of 1.46 for the MNF and 1.41 for the PDMS, respectively.

### Section 6: Measuring the additional optical loss of an MNF caused by PDMS embedding

We measured optical loss of a PDMS embedded MNF by normalising the output intensity with respect to the input intensity within the VIS-NIR spectral range. A broadband light from a tungsten halide lamp (SLS201L, Thorlabs) was coupled into the MNF and the transmission light was directed into a spectrometer (Maya2000 Pro, Ocean optics). As a typical case, the transmission spectra of a 1.5-μm-diameter MNF before and after being embedded in PDMS are shown in Fig. S2(a). Fig. S2(b) gives the wavelength-dependent transmission loss obtained from Fig. S2(a), showing a typical embedding-induced additional loss less than 3 dB within the VIS-NIR spectral range, which is acceptable for optical sensing in this work.

### Section 7: Modeling the power distribution outside the MNF

By solving Maxwell's equations, we obtained the fractional power of the fundamental modes outside the core of a PDMS-embedded silica MNF at 700, 800 and 900 nm wavelength, respectively (Fig. S3). It is clear that decreasing the diameter or increasing the operating wavelength can effectively enhance the fractional power outside the MNF ( $\eta$ ), making the MNF-guided probing light much more sensitive to pressure induced index change and microbending. When we defined the penetration depth of the evanescent field as the length where the field intensity decays to 1/e of the highest intensity outside the MNF, we obtained a penetration depth of about 1.5 μm for an 800-nm-diameter silica MNF at 650-nm-wavelength. Thus, the PDMS film (thickness > 5 μm) is thick enough to enclose the evanescent field of the MNF used in this work.

### Section 8: Calculating the sensitivity and detection limit of the SLWOS

In order to obtain a very small pressure for SLWOS testing, in this work, we used a syringe pump (KD scientific) and a 50-ml-syringe to generate a stable air flow at a flow rate from 5 to 50 ml/min. The relationship between the flow rate and the pressure (measured as weight in the calibration) was calibrated by using a balance (METTLER TOLEDO, ME204E) with a resolution of 0.1 mg (Fig. S5(a)). The weight measured by the balance shows a good linear response to the flow rate (Fig. S5(b)). Note that the gap between the nozzle of the air tube and the tray of the balance was kept a constant value of 100 μm during the calibration and testing by using a 3-D translation stage. As the tube was close to the PDMS surface, we assume the area of contact on the PDMS surface was equal to the inner cross section of the tube, which was about 7 mm<sup>2</sup> for a tube with 3 mm inner diameter. When the air flow rate was 10 ml/min, the measured weight was 0.14 mg, and thus we obtained the pressure  $P \sim 0.2$  Pa. Similarly, with flow rate of 5 mL/min, the pressure was  $\sim 0.1$  Pa.

The sensitivity of our pressure sensor was defined as  $S = \Delta I / I_0 / \Delta P$ , where  $\Delta I$  is the relative change in output intensity,  $I_0$  is intensity of the sensor under no load and  $\Delta P$  is the change in applied pressure. As shown in Fig. S5(d), when the pressure was relatively small, increasing the pressure from 0 to 0.2 Pa (i.e.,  $\Delta P = 0.2$  Pa) caused a  $\Delta I = 37.4\%$ , resulting in a sensitivity  $S = (37.4/100)/0.2 \times 10^{-3} \text{ kPa} = 1870 \text{ kPa}^{-1}$ . Beyond 0.2 Pa, the sensitivity reduced, e.g., with  $P \sim 1$  Pa,  $S \sim 224 \text{ kPa}^{-1}$ .

The low end detection limit was calculated by dividing the pressure of the air flow (0.2 Pa) by the signal-to-noise ratio in Fig. 3(c). It could be observed that the average change in transmission by the air flow of 10 ml/min was 37.4%, and the noise (standard deviation) was 1.3% with a signal-to-noise ratio of  $\sim 29$ . Thus we estimated the low end detection limit to be  $0.2/29 \text{ Pa} \sim 7 \text{ mPa}$ .

### Section 9: Measuring response time of a SLWOS

We measured response time of a SLWOS by using a commercial available ultrasonic cell disruptor (Branson Digital Sonifer 450, frequency: 20,000 Hz) or a home-built vibration test platform (maximum frequency: 4,000 Hz), which was composed of a vibration actuator, a power amplifier and a signal generator (iPhone APP, Signal generator). As shown in Fig. S6, a SLWOS was attached on a glass slide, and the glass slide was mounted on the bottom of a metal frame which was connected with a 3-D translation stage. The output signal was recorded by an oscilloscope.

### Section 10: Characterization of data glove and SLWOSs embedded with 2×2 MNF arrays

For characterization of the data glove (Fig. 4(a)) and SLWOSs embedded with 2×2 MNF arrays (Fig. 4(d)), we employed an LED-CCD system for multichannel sensing. In this case, the light from an LED (central wavelength of 535 nm and FWHM of 35 nm) was simultaneously coupled into input fibers of 5 SLWOSs, with their outputs measured by a calibrated CCD camera (Blackfly BFLY-U3-03S2N-CS, Point Grey Research Inc.). Typically, the intensity of the input light is about 400 nW, measured by an optical power meter (PM100USB, Thorlabs) mounted with a Si photodiode (S120C, Thorlabs). When the gain and exposure time of the CCD camera were set to 1.0 and 10 ms, respectively, bright images of the output fibers can be recorded as shown in Panel T<sub>0</sub> of Fig. 4(f). Since the maximal gain of the camera is 24, it is possible to further reduce the optical power of the LED and couple more fibers with one LED.

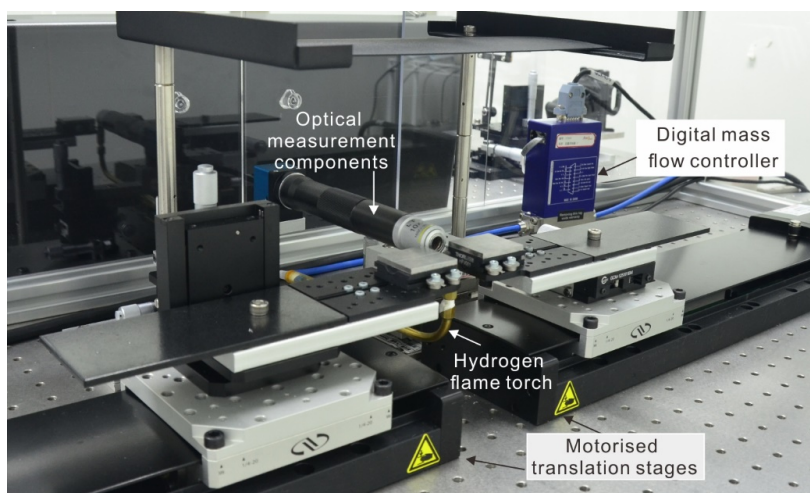


**Fig. S1** | Photograph showing a taper drawing system for MNF fabrication. The taper drawing system consists of a hydrogen flame torch, two motorised translation stages, optical measurement components and a computer.

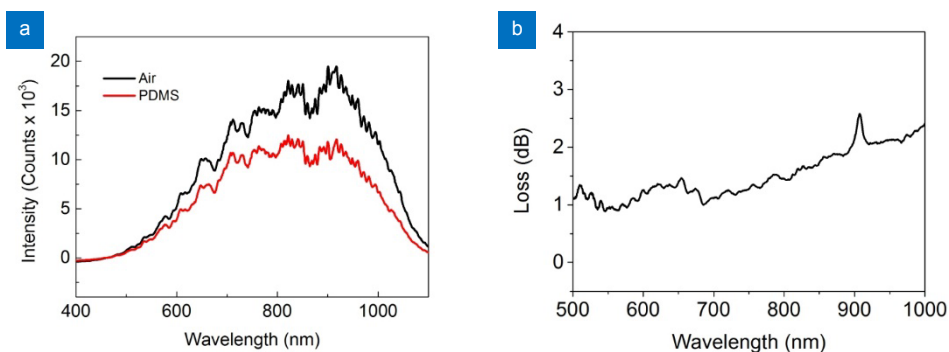


**Fig. S2** | Measurement of the optical loss of a PDMS embedded MNF. (a) Typical transmission spectra of a 1.5- $\mu\text{m}$ -diameter silica MNF before (black line) and after (red line) being embedded in PDMS. (b) Wavelength-dependent transmission loss obtained from Fig. S2(a).

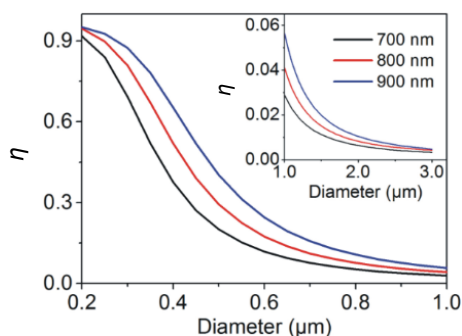


**Fig. S3** | Calculated power distribution outside the MNFs. Fractional power of the fundamental modes outside the core ( $\eta$ ) of PDMS-embedded silica MNFs at 700, 800 and 900 nm wavelength, respectively.

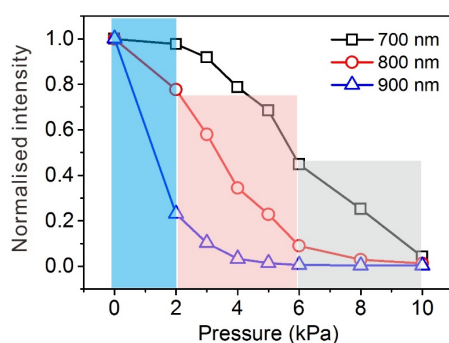


**Fig. S4 | Normalized pressure response of a SLWOS measured at three wavelengths.** The maximum response of different wavelength within different pressure range indicates that, by using broadband probing light, and connecting the pressure response at different wavelength in cascade, e.g., 0–2 kPa, 2–6 kPa and 6–10 kPa at 900, 800 and 700-nm wavelength, respectively, it is possible to expand dynamic range without sacrificing the sensitivity.

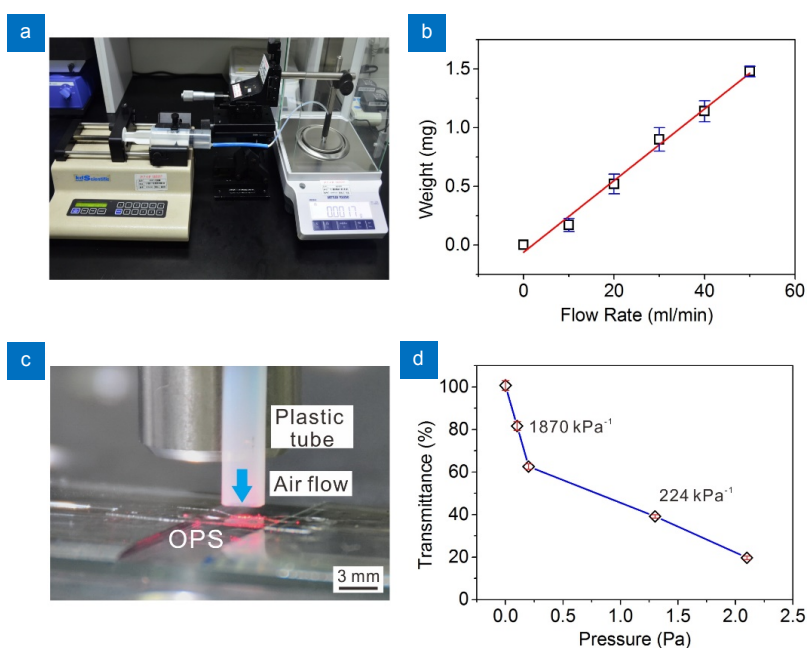


**Fig. S5 | Calibration and measurement of the air flow pressure.** (a) Experimental setup for calibrating the air flow pressure by the weight readout from a balance (METTLER TOLEDO, ME204E). (b) Calibration curve of the flow rate versus the weight. (c) A photograph showing an air flow tube and a suspended SLWOS. (d) Measured optical transmission intensity of the SLWOS under low pressure.

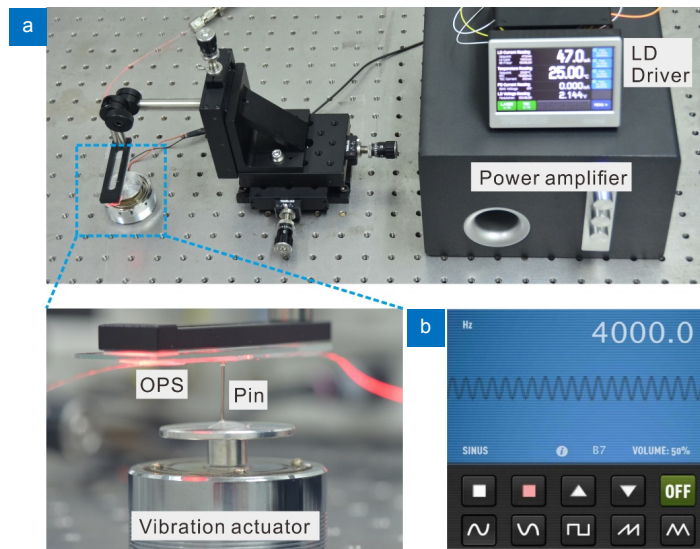


**Fig. S6 | Experimental setup for investigating response time.** (a) A photograph showing the home-built vibration device. (b) Main operation panel of the iPhone based signal generator.

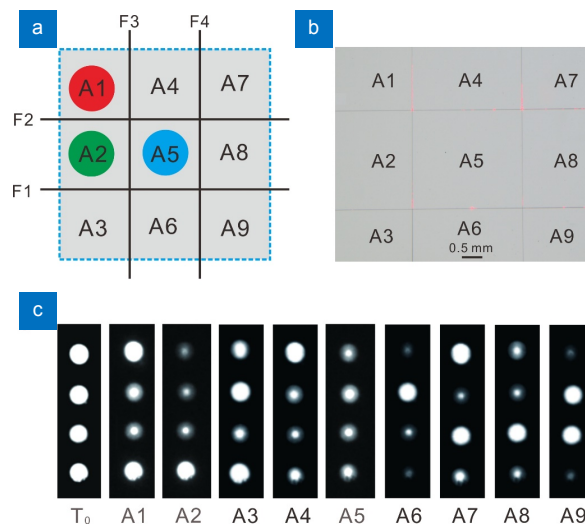


**Fig. S7 | Logic functionality of a SLWOS with 3 mm MNF separation.** (a) Schematic of the sensing areas for tactile sensing. (b) A photograph showing the 2x2 MNF array with 3 mm MNF separation. (c) Images of the endfaces of the four output fibers. When the separation between the two parallel MNFs was 3 mm, the sensitive areas can be identified as 9 grid meshes. As expected, when a pressure was applied on a certain mesh, the surrounding MNFs (2 for corner, 3 for side, and 4 for central square, respectively) give low outputs, while the others keep high, confirming the logic functionality of the SLWOS for spatially denser tactile sensing.

**Table S1 | True value table of the logic output of the 2×2 MNF array with a separation of 1.5 cm.**

Sensing areas	Output of the fibers			
	F1	F2	F3	F4
A	1	0	0	1
B	0	1	0	1
C	1	0	1	0
D	0	1	1	0

**Table S2 | True value table of the logic output of the 2×2 MNF array with a separation of 3 mm.**

Grid meshes	Output of the fibers			
	F1	F2	F3	F4
A1	1	0	0	1
A2	0	0	0	1
A3	0	1	0	1
A4	0	1	1	0
A5	0	0	0	0
A6	0	1	0	0
A7	1	0	1	0
A8	0	0	1	0
A9	0	1	1	0

### Movie S1 | Response of a SLWOS to finger actions

Broadband light from a tungsten halide lamp (Thorlabs, SLS201L) was coupled into a SLWOS (200- $\mu\text{m}$  thickness, 1.2- $\mu\text{m}$ -diameter microfiber). The real time transmission at 700-nm-wavelength was recorded by a spectrometer (Ocean optics, Maya2000 Pro). We investigated response of the SLWOS to three finger actions, named as “tapping”, “non-contact movement”, and “dragging”. The measurement results were shown in Fig. 2(e). Compared to capacitive pressure sensor, the EMI-free SLWOS can effectively avoid unintended operation.

### Movie S2 | Operating a SLWOS in conductive liquid

A SLWOS was put into a petri dish containing conductive blue aqueous solution (NaCl and food dye). When a finger taps the SLWOS successively, corresponding dips were obtained as expected, indicating that the SLWOS can be operated in a conductive environment.

### Movie S3 | Operating a mechanical hand via a five-sensor data glove

A program was used to read the data (bending angles) from the optical data glove and send commands to control the movements of each finger of the mechanical hand. The LED and CCD camera were packaged in the small box, which was strapped to the tester’s forearm.

## References

- Xu Y X, Fang W, Tong L M. Real-time control of micro/nanofiber waist diameter with ultrahigh accuracy and precision. *Opt Express* **25**, 10434–10440 (2017).
- Taflove A H, Susan C. *Computational Electrodynamics: The Finite-Difference Time-Domain Method* (Artech House: Boston, MA, 2000).